iJRASET
International Journal For Research in Applied Science and Engineering Technology

INTERNATIONAL JOURNAL FOR RESEARCH

IN APPLIED SCIENCE & ENGINEERING TECHNOLOGY

Volume: 8 **Issue:** VIII **Month of publication:** August 2020

DOI: https://doi.org/10.22214/ijraset.2020.30971

www.ijraset.com

Call: 08813907089 | E-mail ID: ijraset@gmail.com

International Journal for Research in Applied Science & Engineering Technology (IJRASET)
ISSN: 2321-9653; IC Value: 45.98; SJ Impact Factor: 7.429
Volume 8 Issue VIII Aug 2020- Available at www.ijraset.com

Rapid Detection of COVID 19 via Surface Enhanced Raman Spectroscopy

Asma M. Elsharif
Department of Chemistry, College of Science, Imam Abdulrahman Bin Faisal University, P.O. Box 1982, Dammam 31441, Saudi Arabia

Abstract: Coronavirus Disease-2019, known as COVID-19, has been declared a public health emergency of worldwide concern [1-4]. This paper reports a new design of Surface Enhance Raman Spectroscopy (SERS) substrate that can deliver higher sensitivity and the closest interaction to the target structure of the hot spots for the immunomagnetic capturing based concentration method. This substrate contains Polydimethylsiloxane (PDMS) inverted nanocavity arrays, which can funnel the light to the top where plasmonic gold nanorods occur. A high reflective and low loss layer is deposited at the outer surface, which reflects the photons multiple times and hence the number of photons is increased. After monitoring the consistent pattern and geometric shape of inverted cavities, the hot spots of the suggested Surface Enhance Raman Spectroscopy (SERS) substrate might have improved influence of 10^{10} or even higher, which could be sufficient to discover the immunomagnetically densified virus.
Raman spectroscopy is a promising candidate in virus diagnosis given its fast and label-free nature, so long as the concentration of the pathogen is high enough to provide reasonable sensitivity [5-9].
Keyword: COVID 19, Plasmonic hot carrier collection, Gold nanorods, SERS, nanocavity arrays, PDMS.

I. INTRODUCTION

Surface Enhanced Raman Spectroscopy (SERS) technique is an operational biosensors technique that could make the sensitivity of the pathogen more rapid [5-9]. Scattering photons deliver chemical information in the form of vibrational rays to other chemical bonds with the highest spatial resolution [10]. However, as the inelastic scattering signals are very weak, Raman scattering cannot be ideal for the identification of chemicals unless these signals are enhanced effectively. The vital idea in creating SERS is to generate the ideal metal surface. In addition to this, it has also been discovered that SERS mainly depends on the kind of metal and the roughness of the surface of that metal, and consequently, the major concern of this process is to prepare the substrate [10].
The main purpose of imposing SERS into the minimum concentration of bio-sensing is to enhance the intensity level of the vibration mode, I_{SERS} through increasing the electric field at the location of the sensing [[10]].

$$I_{SERS} \propto \left|\frac{E(\lambda)}{E_0(\lambda)}\right|^2 \left|\frac{E(\lambda_s)}{E_0(\lambda_s)}\right|^2 \quad (1)$$

Where λ is the incident wavelength and $\lambda_s$represents the Raman scattering wavelength, E signifies the local electric field intensity; E_0 is incident electric field intensity. As the frequency shift due to Raman scattering is smaller than the incident wavelength, the enhancement factor (EF) is shown as [[11]]:

$$E \propto \left|\frac{E(\lambda)}{E_0(\lambda)}\right|^4 \quad (2)$$

With the provided order of magnitude enhancement on the light field, the signal output of a substrate is:

$$I \propto EF \times N_{molecule} \quad (3)$$

Where, $N_{molecule}$ characterizes the number of molecules in relation to the plasmonic "hot-spot".
The most common method to enhance the EF factor of a substrate is to use plasmonic nanomaterial that can provide the localized surface plasmon attribute (LSPR) [7]. In LSPR, the surface plasmon will connect with the photon, which is too close to the surface of the metal, restraining the light field within a small range and increasing light field intensity.
Within the typical detection, the pathogen concentration is as small as 1-100 CFU/mL, and the pathogen must be enhanced by 10^5 to accomplish Raman measurements [[12], [13]]. So according to this situation, the performance of the Raman enhancement approach is to put control on the local electromagnetic environment of plasmonic deposition, along with the intention of increasing the concentration of photons through which the metal deposition can take.

ISSN: 2321-9653; IC Value: 45.98; SJ Impact Factor: 7.429
Volume 8 Issue VIII Aug 2020- Available at www.ijraset.com

Weisheng et al. [[15]] suggest placing the gold dimers on a metallic surface. The metal surface creates the plasmon and restrains the light field. The dimers receive the photons from the focused light field and the EF is about 10^5. Masahiko et al. [[15]] use Au disc array on a dielectric-metal-quartz substrate. The periodic disc array scatters lights into wave pack whose wavevector matches the plasmon mode between dielectric and metal, and photons are trapped and delivered to the discs. In this work, the EF rises to 10^6. Dongzhi et al. [[16]] have said to place the metallic film on oxidized porous Al. The Al_2O_3 layer between the substrate and metallic film will perform as the function of the resonator that records the light, which enhances the EF created by the metal film at the topmost structure, resulting in an EF of 10^4. Still, the enhancement of a single nanorod can reach 10^6 if associated accurately with incident light.

Immunomagnetic capturing is one of the famous methods to concentrate pathogens, which permits two to three orders of magnitude upgrading of the pathogen. Moreover, the pathogen will be connected by the antibiotic modified magnetic bead. The magnetic field can be utilized to collect the pathogen-bead clusters [18-20]. Further, for the purpose of performing rapidly the non-culturing discovery of the pathogen, Raman sensor sensitivity should be upgraded in a more effective way. But the purpose of Raman measurements cannot be considered to fulfill this sensitivity gap. The trapped pathogen will be transmitted to the Raman substrate as in a substrate approach [[14]-[16]], or can be directly reconnected to the plasmonic nanoparticles recognized as a colloidal method [[17]-[19]]. The colloidal method is intended to stimulate the particles of LSPR, whose EF is restricted to 10^6. Moreover, with the support of an ordered surface structure, the EF contained in the substrate can be barely increased more than $10^{6.}$

Within the colloidal approach, bead, nano metallic particles, and pathogens are rarely connected to each other, and incident light can be restricted by those target cells, mostly if they are covered by the target cells. In the substrate method, pathogens will stand on the surface of plasmonic and incident light will be transmitted from the bottom to the top. Along with that, a huge portion of the incident light will be blocked/absorbed by the target cells and small number of photons can reach out to the plasmonic metal.

II. FDTD SIMULATION

The SERS substrate determined in this paper is to make series transparent inverted nanocavity arrays from which a radius reduces beside the path of light. A reflectively high and bottom layer of the nanocavity series is covered with a reflected particle. In this context, these particles are multi-layered or reflected, which are known as photons. These are increased in density by an outside layer with a density of 5-10 times each. When this higher concentration of “photon gas” reaches the plasmonic metal, the Raman signal enhancement can be as high as 10^8. Furthermore, the substrate is premeditated, which allows the light particles to transparently enter the bottom surface along with the non-photon particles to interrupt the process.

The incident photons are multi-reflected inside the cavity, known as cavity resonance. The intended resonance can capture light and concentrate it. In this work, the capturing of photons inside the structured cavity is utilized to demonstrate SERS along with the concentrated absorption of the photon. The numerical method used in this paper is Finite-Difference Time-Domain (FDTD) method, conducted by FDTD Solution (Lumerical Inc.) with 3nm cubic mesh. In the simulation, 2-D arrays of meshes have been utilized as observing planes, and the SERS refers to the maximum field enhancement in the observing plane. The ground surface of the substrate can be stated as Polydimethylsiloxane (PDMS) along with the light material used from top to bottom. A coated film in this procedure is utilized to enhance the substrate while the photons reflections can be enabled at EF 10^{10}. The effected enhancement occurs only when the inverted cavity top surface is decreased due to the sloping of the cavity. Similarly, the gap between the two inverted cavity series must be enough to cover the magnetic beads, which can create the contact lesser.

By pouring liquid PDMS onto the structure and letting it cool down, the microstructure pattern can be transferred into a new structure. The geometric features of inverse cavity are bottom diameter 500 nm, top diameter 200 nm, height 1000 nm and periodicity 840 nm. Note this set of geometry is subject to change in the second section of the designing process [21, 22].

In the FDTD simulation, all structures are surrounded by water, and materials’ optical models are obtained from Palik’s book [23].

III. RESULTS AND DISCUSSION

A 20 nm film is made on the surface of the inverse cavity, except the top. A plane wave source illuminates normally from the bottom base to the top. The incident electric field is parallel to the axis of the nanorod to excite LSPR. Because of this, the vertical axis electronic field is rounded with the nanorod so that the LSPR is not prompted with the entire structure; thus this transformation would not be comprehended. A 15nm diameter along with the length of the axis at 45nm Au nanorod will be used in the simulation, as it was previously used [24, 25, 26]. We are particularly interested in the field enhancement at the top of cavity, as in a real bio-sensing experiment, the top of the inverse cavity will be the most possible touching point of the structure and analyte. To better elucidate the role of the cavity’s photon capturing to enhance the nanorod’s LSPR, there is only one nanorod at the top of inverse cavity.

ISSN: 2321-9653; IC Value: 45.98; SJ Impact Factor: 7.429
Volume 8 Issue VIII Aug 2020- Available at www.ijraset.com

Distribution of the electromagnetic field in a cross section of structures along the axis of the nanorod will also be used in this work. In the flat PDMS surface and nanorod case, a layer of Au nanorods has been deposited at a flat PDMS surface, with the separation of every nanorod at 850 nm. A flat PDMS surface case stands for the commercial Raman substrate and will serve as the standard of comparison.

In order to prompt the resonated cavity, a higher level reflected interior cavity is needed. According to Fresnel's equations, a high reflection occurs when the refractive indexes of two interface materials are large [27]. Si and Au are chosen as coated films.

Because the refractive index for PDMS in the visible region is around 1.4, Au with an index around 0.3 and Si with an index around 4 are chosen as coating material. But due to the metallic nature of Au, the optical loss of the Au coated cavity can be high. The power dissipating profile of Si and Au deposited cavity are shown in Figure 1a and Figure 1b, in the cross section. The power dissipation can be defined as [28], which is directly correlated with light energy density [29]:

$$w(x,z) = \frac{1}{2}\varepsilon_0 \omega \varepsilon''(x,z)\left|\vec{E}(x,z)\right|^2 \tag{4}$$

In Fig. 1a and Fig. 1b, photon energy is mostly dissipated in the film for both Si and Au coated cases. But the intensity in the Au coated case is nearly 750 times larger than with Si film. Fig. 1c and Fig. 1d show the electric field intensity. In Fig. 1c, with Si coated, the electric field is enhanced around the top of cavity. With a gradually narrowing cavity and low optical loss, the photons are concentrated and delivered to the top of the cavity structure. In Fig. 1d, the electric field is enhanced at the side wall of the cavity, and the photons are dissipated and scattered at the cavity, before going to the top. Even photons are concentrated in a similar level in two cases, but the dissipation effect will create immense modification.

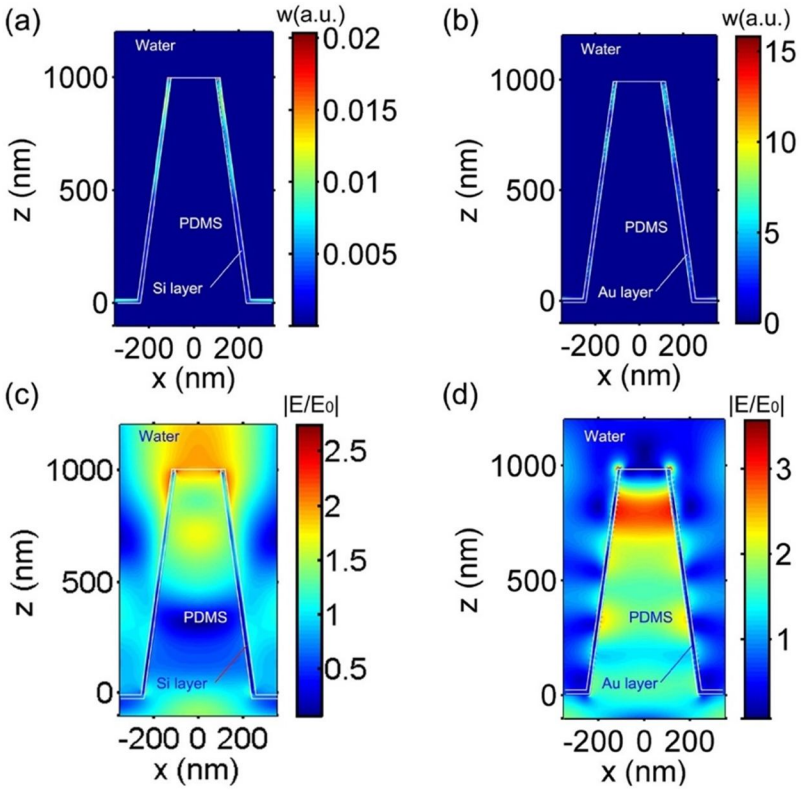

Figure 1: 758nm power dissipation distribution for cross sections of (a) SiCN without nanorod (b) AuCN without nanorod. 758nm electric distribution for cross sections of (c) SiCN without nanorod (d) AuCN without nanorod.

Figure 2a and Fig. 2b show the 758nm field distribution in Si and Au coated inverted nanocavity with nanorod at the tops. The cross section is illustrated in Fig. 2d. Note that the top is free of coating to ensure that concentrated photons will not be reflected by the interface. In Fig. 2a, the electric field is highly confined around the nanorod, the top of the inverted structure. Inside the cavity, the electric vectors exhibit a multi-reflection resonance pattern, exactly the cavity resonance mode. In Fig. 2b, the electric field is also highly confined around the nanorod. In Fig. 2a and Fig. 2b, it can be seen that the enhancement patterns are exactly same, but the intensities are different.

But with the help of Si film, the electric field enhancement can be improved nearly 5 times that of the Au coated case. Fig. 2c shows the SERS as a function of wavelength at the top observing plane for Si coated, Au coated and flat surface cases. One can see at 758nm, the SERS reaches 10^8 for the Si coated case, 10^6 for the flat surface case and 10^3 for the Au coated case. With the help of a low-loss photon-concentrated Si coated cavity, the SERS can be improved by 10^2. However, even with the assistance of the cavity, the Au loss reduces the SERS a lot, making field enhancement lower than isolated LSPR.

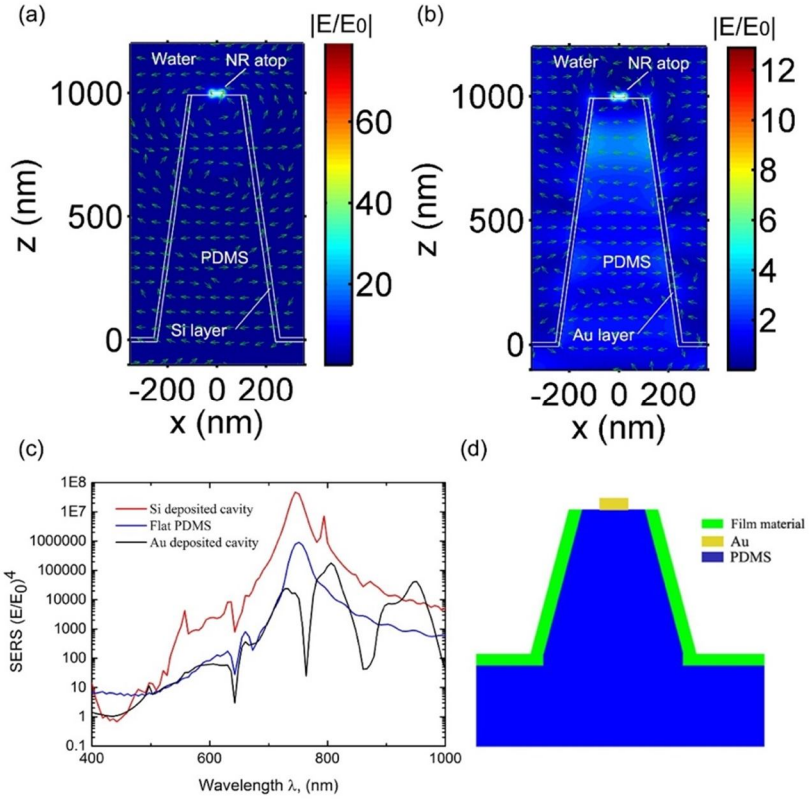

Figure 2: 758nm electric field in cross sections of (a) Si (b) Au deposited inverse cavity without nanorod. (c) SERS spectrum for 3 related structures. (d) Illustration of cross section of the proposed structure.

In order to analyze the optimum bottom and slope inverted nanocavity diameter, the comparative concentration $I_{relative}$ has a correlation [[10]]:

$$I_{relative} \propto \sum EF_{top} \times N_{molecule} \tag{5}$$

$N_{molecule}$ is the molecules number at the top surface, and is comparative high range S_{top}. The enhancement at the top EF_{top} is certainly connected to the inverted cavity slope whereas S_{top} is adversely linked. For finding the tradeoff amid EF_{top} and S_{top}, a function is described as:

$$f_{inverted\ cavity} = \frac{EF_{top} \times S_{top}}{\sum S_i} \tag{6}$$

Where $\sum S_i$ is the total area that a single cavity averagely takes. This function is actually the ratio between signal intensity of inverted nanocavity arrays to flat surface under the same rod deposition density. For the flat top area f = 1, and for our first harvesting nano cavity prepared combination f = 1. The determination is to max out f. The EF_{top} is premeditated via:

$$\sqrt{EF_{top}} = \frac{S_{top} + (\pi D^2 - S_{top}) \times \bar{R}(0.5\pi - \theta)}{S_{top}} \tag{7}$$

$\bar{R}$ is the polarization averaged reflection of the film, obtained from Fresnel's equation. In the calculation, given that the film thickness is 15nm and much smaller than the wavelength in the film, thin film limit is introduced where wavevectors in PDMS and water are close to free space and wave vector in film is nearly independent of radius a [30-33].

IV. CONCLUSION

In this work, an SERS substrate is proposed for the rapid diagnosis of COVID-19. The high sensitivity originates from the combination of photon funneling, dense packing and an optimized inverted nanocavity. 15nm thick Si film is deposited at the surface of the inverted cavity structure, which has high reflection and a low loss concentrating of photons. The Raman enhancement factor is increased by 2 orders of magnitude, while only reducing contact area by 1 order and making the overall sensitivity 1 order higher as compared with the rough surface approach. The Si coated structure proposed in this paper has the advantages of low-cost and large-scale productivity, and fits immunomagnetic pathogen collecting well. This work will facilitate the development of novel optical bio-substrate along with fast and precise pathogen diagnosis.

V. ACKNOWLEDGMENTS

The author gratefully acknowledges the use of the service and facilities of Imam Abdulrahman Bin Faisal University.

REFERENCES

[1] Cortegiani A, Ingoglia G, Ippolito M, Giarratano A, Einav S (2020) A systematic review on the efficacy and safety of chloroquine for the treatment of COVID-19. Journal of Critical Care 57
[2] Wu Z, McGoogan JM (2020) Characteristics of and important lessons from the coronavirus disease 2019 (COVID-19) outbreak in China: summary of a report of 72 314 cases from the Chinese Center for Disease Control and Prevention. Jama
[3] Savarino A, Boelaert JR, Cassone A, Majori G, Cauda R (2003) Effects of chloroquine on viral infections: an old drug against today's diseases. Lancet Infect Dis 3: 722–7
[4] Colson P, Rolain JM, Raoult D (2020) Chloroquine for the 2019 novel coronavirus SARS CoV-Int. J. Antimicrob Agents 105923
[5] Assad ON, Gilboa T, Spitzberg J, Juhasz M, Weinhold E, Meller A (2017) Light-enhancing plasmonic-nanopore biosubstrate for superior single-molecule detection. Advanced Materials 29: 1605442
[6] Yanik AA, Cetin AE, Huang M, Artar A, Mousavi SH, Khanikaev A, et al (2011) Seeing protein monolayers with naked eye through plasmonic fano resonances. Proceedings of the National Academy of Sciences of the United States of America 108: 11784-11789
[7] Lee KL, Huang JB, Chang JW, Wu SH, Wei PK (2015) Ultrasensitive biosubstrates using enhanced fano resonances in capped gold nanoslit arrays. Scientific Reports 5: 8547
[8] Chen CK, Li CT, Yen TJ, Lai YC, Chang YT (2010) A multi-functional plasmonic biosubstrate. Optics Express 18: 9561-9569
[9] Kim K, Yoon JK (2005) Raman scattering of 4-aminobenzenethiol sandwiched between ag/au nanoparticle and macroscopically smooth au substrate. Journal of Physical Chemistry B 109: 20731-6
[10] Xu W, Ling X, Xiao J, Dresselhaus MS, Kong J, Xu H, et al (2012) Surface enhanced Raman spectroscopy on a flat graphene surface. Proceedings of the National Academy of Sciences of the United States of America 109: 9281-6
[11] Tao AR, Yang P (2005) Polarized surface-enhanced Raman spectroscopy on coupled metallic nanowires. Journal of Physical Chemistry B 109: 15687
[12] Shen HX, Zou WJ, Yang ZL, Yuan YX, Xu MM, Yao JL, Gu RA (2015) Surface-enhanced Raman spectroscopy on single fe2o3@au spindle nanoparticle: polarization dependence and fdtd simulation. Journal of Optics 17: 114014
[13] Puttaswamy S, Lee BD, Sengupta S (2011) Novel electrical method for early detection of viable bacteria in blood cultures. Journal of clinical microbiology 49: 2286-2289
[14] Premasiri WR, Sauer-Budge AF, Lee JC, Klapperich CM, Ziegler LD (2012) Rapid bacterial diagnostics via surface enhanced Raman microscopy. Spectroscopy (Springfield, Or.) 27: 8-31
[15] Yue, W, Wang Z, Whittaker J, Lopez-royo F, Yang Y, Zayats AV (2017) Amplification of surface-enhanced Raman scattering due to substrate-mediated localized surface plasmons in gold nanodimers. Journal of Materials Chemistry C 5: 4075-4084
[16] Shioi M, Jans H, Lodewijks K, Dorpe PV, Lagae L, Kawamura T (2014) Tuning the interaction between propagating and localized surface plasmons for surface enhanced Raman scattering in water for biomedical and environmental applications. Applied Physics Letters 104: 243102
[17] Shan D, Huang L, Li X, Zhang W, Wang J, Cheng L, Feng X, Liu Y, Zhu J, Zhang Y (2014) Surface plasmon resonance and interference coenhanced SERS substrate of AAO/Al-based Ag nanostructure arrays. The Journal of Physical Chemistry C 118: 23930-23936
[18] Wang J, Wu X, Wang C, Shao N, Dong P, Xiao R, Wang S (2015) Magnetically assisted surface-enhanced Raman spectroscopy for the detection of Staphylococcus aureus based on aptamer recognition. ACS applied materials & interfaces 7: 20919-20929
[19] Sha MY, Xu H, Natan MJ, Cromer R (2008) Surface-enhanced Raman scattering tags for rapid and homogeneous detection of circulating tumor cells in the presence of human whole blood. Journal of the American Chemical Society 130: 17214-17215
[20] Lesaicherre ML, Paxon TL, Mondello FJ, Burrell MC, Linsebigler A (2009) Portable Raman instrument for rapid biological agent detection and identification. Next-Generation Spectroscopic Technologies, International Society for Optics and Photonics 7319
[21] Chou JB, Li XH, Wang Y, Fenning DP, Elfaer A, Viegas J, Kim SG (2016) Surface plasmon assisted hot electron collection in wafer-scale metallic-semiconductor photonic crystals. Optics express 24: A1234-A1244
[22] Chou JB, Yeng YX, Lee YE, Lenert A, Rinnerbauer V, Celanovic I, et al (2014) Enabling ideal selective solar absorption with 2d metallic dielectric photonic crystals. Advanced Materials 26: 8041
[23] Palik E D (1998) Handbook of optical constants of solids
[24] Chou JB, Fenning DP, Wang Y, Polanco MAM, Hwang J, El-Faer A, Sammoura F, Viegas J, Rasras M, Kolpak AM (2015) Broadband photoelectric hot carrier collection with wafer-scale metallic-semiconductor photonic crystals. Photovoltaic Specialist Conference (PVSC) IEEE 42nd: 1-6
[25] Elsharif AM (2018) The Effect of the Electron Tunneling on the Photoelectric Hot Electrons Generation in Metallic-Semiconductor Nanostructures. Chemical Physics Letter 691: 224-230

[26] Elfaer AM, Wang Y, Li XH, Chou JB, Kim SG (2016) Gold Nanorods Coated Metallic Photonic Crystal for Enhanced Hot Electron Transfer in Electrochemical Cells. MRS Advances 1: 831-837
[27] Zhang Z (2007) M. Nano/microscale heat transfer (McGraw-Hill, New York
[28] Zhao B, Zhao JM, Zhang ZM (2014) Enhancement of near-infrared absorption in graphene with metal gratings. Applied Physics Letters 105: 031905
[29] Jia, Z-X, Shual Y, Guo Y-M, Tan H-P (2017) Nanoparticle-crystal towards an absorbing meta-coating. Optics express 25: A375-A390.
[30] Hosseini P, Abidi SZ, Du E, Papageorgiou DP, Choi Y, Park Y, Higgins JM, Kato GJ, Suresh S, Dao M, Yaqoob Z, So PT (2016) Cellular normoxic biophysical markers of hydroxyurea treatment in sickle cell disease. Proceedings of the National Academy of Sciences 113: 9527-9532.
[31] Abu-Lail NI, Camesano TA (2006) The effect of solvent polarity on the molecular surface properties and adhesion of Escherichia coli. Colloids and Surfaces B: Biointerfaces 51: 62-70.
[32] Lee, CS, Shung-Wu L, Shun-Lien C (1986) Normal modes in an overmoded circular waveguide coated with lossy material. IEEE transactions on microwave theory and techniques 34: 773-785.
[33] Elsharif AM (2020) Geometry and Polarization Effects in Designing Metallic-Semiconductor Nanostructures for Plasmonic Hot Carrier Collection. Plasmonics.

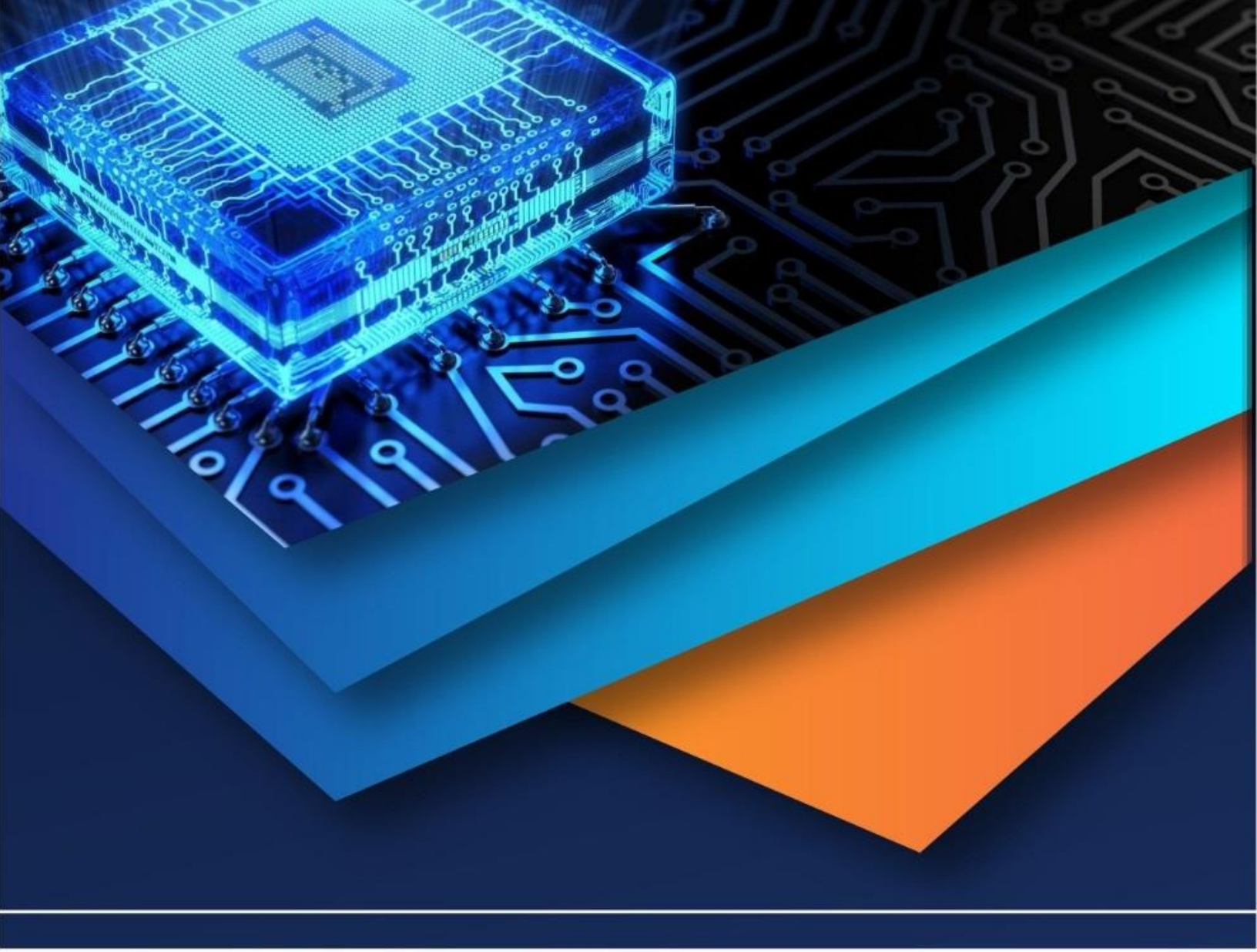

10.22214/IJRASET

45.98

IMPACT FACTOR: 7.129

IMPACT FACTOR: 7.429

INTERNATIONAL JOURNAL FOR RESEARCH

IN APPLIED SCIENCE & ENGINEERING TECHNOLOGY